Annual net community production in the subtropical Pacific Ocean from in situ oxygen measurements on profiling floats

Bo Yang[1] (ID), **Steven R. Emerson**[1] (ID), and **Seth M. Bushinsky**[2] (ID)

[1]School of Oceanography, University of Washington, Seattle, Washington, USA, [2]Atmospheric and Oceanic Sciences, Princeton University, Princeton, New Jersey, USA

Abstract Annual net community production (ANCP) in the subtropical Pacific Ocean was determined by using annual oxygen measurements from Argo profiling floats with an upper water column oxygen mass balance model. ANCP was determined to be from 2.0 to 2.4 mol C m^{-2} yr^{-1} in the western subtropical North Pacific, 2.4 mol C m^{-2} yr^{-1} in the eastern subtropical North Pacific, and near zero in the subtropical South Pacific. Error analysis with the main sources of uncertainty being the accuracy of oxygen measurements and the parameterization of bubble fluxes in winter suggested an uncertainty of ~0.3 mol C m^{-2} yr^{-1} in subtropical Pacific. The results are in good agreement with previous observations in locations where ANCP has been determined before. These are the first results from the western subtropical North Pacific and subtropical South Pacific where ANCP have not been evaluated before. ANCP for the subtropical South Pacific is significantly lower than in all other open ocean locations where it has been determined by mass balance. Comparison of our observations with net biological carbon export estimated from remote sensing algorithms indicates that observations from the subtropical North Pacific are higher than the satellite estimates, but those in the subtropical South Pacific are lower than satellite-determined carbon export.

1. Introduction

Export of organic carbon from the surface ocean to depth, known as the "biological pump," plays an important role in global carbon cycle. It helps maintain the pCO_2 of the atmosphere by lowering surface-ocean pCO_2 and oxygen minimal zones by influencing oxygen consumption in the ocean thermocline [*Longhurst and Harrison*, 1989; *Hofmann and Schellnhuber*, 2009; *Kwon et al.*, 2009]. In the upper ocean, at steady state over an annual cycle, the flux of biologically produced organic matter to the ocean interior is equal to the annual net community production (ANCP).

The metabolite mass balance approach to measure ANCP comprises a wide range of methods by using different chemical tracers, including time series measurements of dissolved inorganic carbon drawdown [e.g., *Lee*, 2001; *Fassbender et al.*, 2016], nitrate drawdown [e.g., *Wong et al.*, 2002; *Plant et al.*, 2016], O_2/N_2 ratio [e.g., *Emerson et al.*, 2008], O_2/Ar ratio [e.g., *Craig and Hayward*, 1987; *Emerson et al.*, 1991; *Cassar et al.*, 2015], and carbon isotope mass balance [e.g., *Quay et al.*, 2009]. In the past decade, development of autonomous sensor platforms like the gliders and Argo floats made it possible to perform long-term monitoring of chemical tracers like O_2 and nitrate [e.g., *Bushinsky and Emerson*, 2015; *Nicholson et al.*, 2008; *Plant et al.*, 2016; *Riser and Johnson*, 2008], which avoids the traditional extrapolation uncertainties from using the summer-only data and allows more accurate estimate of ANCP.

Global estimates of ANCP have been obtained mainly by using two methods: global circulation models [e.g., *Bopp et al.*, 2001] and satellite-based remote sensing observations [e.g., *Siegel et al.*, 2014; *Westberry et al.*, 2012]. However, both model and remote sensing approaches still rely on the field data for model/algorithm development and for calibration purposes. *Emerson* [2014] argued that both model and satellite-determined ANCP are far more geographically variable than experimental measurements. For example, ANCP determined from mass balance at the sites of Hawaii Ocean Time-series (HOT), Ocean Station Papa (OSP), and Bermuda Atlantic Time-series study are 2.5, 2.3, and 3.8 mol C m^{-2} yr^{-1}, respectively, while the remote sensing estimates (vertically generalized productivity model) at those sites are 1.4, 4.6, and 1.5 mol C m^{-2} yr^{-1}, respectively. Greater spatial homogeneity is consistent with recent modeling studies that describe the consequences of variable C:P ratios in plankton [*Teng et al.*, 2014; *DeVries and Deutsch*, 2014].

The western subtropical North Pacific and subtropical South Pacific Ocean are oligotrophic regions with very low surface nutrient concentrations [*Garcia et al.*, 2014] and extremely low carbon export as determined by satellite maps [e.g., *Siegel et al.*, 2014; *Westberry et al.*, 2012] and ocean global climate models (GCMs) [e.g., *Bopp et al.*, 2001]. Because ANCP has not been determined experimentally in these extremely oligotrophic regions we deployed three Argo floats in the western subtropical North Pacific (between 17.7–20.2°N and 162–164.5°E, to the southeast of Kuroshio Extension) and one float in the subtropical South Pacific (16.5°S, 161.1°E) to do this. We have previously shown that it is possible to determine ANCP by using Argo float-derived oxygen measurements at Ocean Station Papa (OSP) [*Bushinsky and Emerson*, 2015]. The western subtropical North Pacific study area is influenced by the seasonal cycle of southeast summer monsoon and northeast winter monsoon [*Tomczak and Godfrey*, 1994], suggesting that monsoon-driven physical processes might bring nutrients into the euphotic zone of this area. The subtropical South Pacific study area, on the other hand, is under weak but steady westerlies with little seasonality [*Tomczak and Godfrey*, 1994].

2. Methods

2.1. Data Acquisition

Oxygen, salinity, and temperature data used for ANCP calculation were obtained from five University of Washington (UW) Special Oxygen Sensor Argo floats (SOS-Argo) and an Argo float deployed at the Hawaii Ocean Time-series (HOT) by the float group at Monterey Bay Aquarium Research Institute (MBARI) (Figure 1). All floats were operated at a cycle interval of ~5 days.

The Special Oxygen Sensor Argo (SOS-Argo) floats used in this study were equipped with Aanderaa oxygen optodes (Model 4330, Aanderaa Data Instruments AS, Norway) installed on an ~60 cm long pole attached to the end cap of floats (Figure 1), which avoids the seawater splash during the surface period and allows pure atmospheric pO$_2$ measurements for air calibration. For all SOS-Argo floats, the optode oxygen measurements were calibrated against the air pO$_2$ calculated from optode temperature, National Centers for Environmental Prediction (NCEP) relative humidity, and sea level pressure data products [*Bushinsky et al.*, 2016]. After each profile cycle, when the float reached the surface, the optode measured air pO$_2$ every 2 min for 1 h. Optode air measurements were quality controlled by filtering out data for which the standard deviation of the pO$_2$ measurements over a 10 min period changed by more than 0.2%, air temperature changed by more than 1°C over the air measurement period, or sea level atmosphere pressure changed more than 0.1% during the air measurement period. The mean of the remaining pO$_2$ air measurements from each air period was plotted against the time since deployment to obtain a linear regression for optode calibration. Details of the optode air calibration technique are presented in *Bushinsky et al.* [2016]. The data from this study can be found on our website (https://sites.google.com/a/uw.edu/sosargo/).

Quality-controlled oxygen data for the float at HOT (float F8497) were obtained from MBARI database (http://www.mbari.org/science/upper-ocean-systems/chemical-sensor-group/floatviz/). Because the MBARI float did not have the air calibration mechanism, these data were corrected to ship-based oxygen titrations (0–150 m) from the HOT time series cruises by choosing the Argo profiles obtained within 5 days and 300 km of the HOT ship-board measurements (http://hahana.soest.hawaii.edu/hot/hot-dogs/interface.html).

N$_2$ data determined in surface waters at OSP and used in this paper to calibrate the bubble portion of the gas exchange model were obtained from a gas tension device (GTD) on the OSP mooring (see *Emerson and Stump* [2010] and *Emerson et al.* [2008] for an explanation of the methods used to transform pressure and O$_2$ measurements to N$_2$ concentrations). The O$_2$ and N$_2$ data used here are archived at the Carbon Dioxide Information Analysis Center (http://cdiac.ornl.gov/oceans/Moorings/Papa_145W_50N.html). Wind speed data used to calculate the air-sea gas exchange mass transfer coefficient were obtained from the advanced scatterometer data product (http://apdrc.soest.hawaii.edu/las/v6/). Sea level pressure and relative humidity products used to calibrate the oxygen sensors in air were from National Centers for Environmental Prediction (NCEP) reanalysis (http://www.esrl.noaa.gov/psd/data/gridded/).

The satellite-based net primary production (NPP) estimates and the export production to total primary production ratio (NCP/NPP) were used to calculate remote-sensing-based NCP to compare with our field observations. NPP data were from remote sensing data products (http://www.science.oregonstate.edu/ocean.productivity/index.php), using both the Vertically Generalized Production Model (VGPM) [*Behrenfeld*
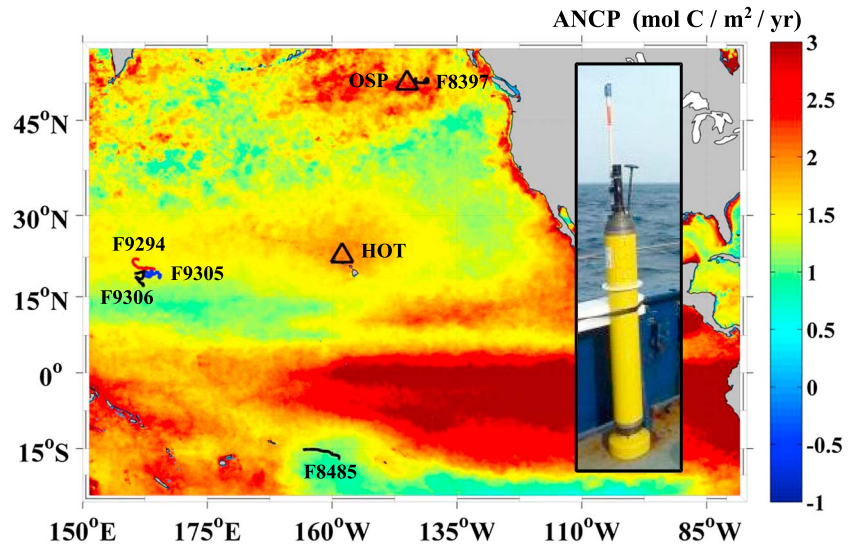
Figure 1. Tracks of Argo floats (black, red, and blue lines) in the Pacific with a background of satellite-determined carbon export from January 2015 to January 2016. Float 8497 (track not shown) was deployed near Hawaii Ocean Time-series (HOT) from 2013 to 2015 in the eastern subtropical North Pacific by Ken Johnson and his colleagues from MBARI. All floats other than F8497 are UW SOS-Argo floats (pictured above) with air-calibrated oxygen sensors. Satellite-based carbon export was calculated with net primary production (NPP) from CbPM algorithm [*Westberry et al.*, 2008, http://www.science. oregonstate.edu/ocean.productivity/index.php] multiplied by the NCP/NPP ratio compiled by *Laws et al.* [2011] (equation (11)). The triangles mark the locations of HOT and OSP: Ocean Station Papa.

and Falkowski*, 1997] and the Carbon-based Production Model (CbPM) [*Westberry et al.*, 2008]. Ancillary data used for calculation of NPP (e.g., sea surface temperature) can be found from the same site. The NCP/NPP ratio (ef-ratio) used was from *Laws et al.* [2011].

2.2. Upper Water Column Oxygen Mass Balance Model

Calibrated oxygen, temperature, salinity, atmospheric pressure, and wind speed data were used in an upper ocean oxygen mass balance model to calculate ANCP. A schematic of the simplified two-layer upper water column oxygen mass balance model used in this study is presented in Figure 2. Horizontal and vertical advections and changes in oxygen supersaturation caused by float drift are assumed to be small compared to air-sea gas exchange, bubble injection, and diapycnal diffusion as demonstrated by *Bushinsky and Emerson* [2015] in their study of OSP data [*Bushinsky and Emerson*, 2015] and as explained in the supporting information. The model used here has just two layers: the upper mixed layer and a deeper layer with the deepest winter mixed layer depth as its base. We define ANCP as the flux of organic carbon that escapes the upper ocean (sum of layers 1 and 2) after completion of the seasonal mixed layer cycle. Organic carbon exported from the shallow summer mixed layer and respired between layers 1 and 2 is not included in ANCP because it can be reventilated to the atmosphere in winter [*Bushinsky and Emerson*, 2015; *Körtzinger et al.*, 2008; *Palevsky et al.*, 2016b].

Oxygen concentration changes in layer 1 are controlled by gas exchange fluxes, which include both the air-sea interface diffusion (F_S) and bubble processes (F_B), entrainment of waters from layer 2 to the upper mixed layer (F_E), and net biological oxygen production (J_1).

$$\frac{d(h_1[O_2])}{dt} = F_S + F_B + F_E + J_1 \qquad \text{mol m}^{-2} \text{ d}^{-1} \qquad (1)$$

Oxygen change in layer 2 is a result of entrainment (F_E), diapycnal eddy diffusion across the base of layer 2 (F_{Kz}), and net biological oxygen production (J_2).

$$\frac{d(h_2[O_2])}{dt} = F_E + F_{Kz} + J_2 \qquad \text{mol m}^{-2}\text{d}^{-1} \qquad (2)$$

The sum of J_1 and J_2 is the total net biological oxygen production (equation (3)) in the upper water column.
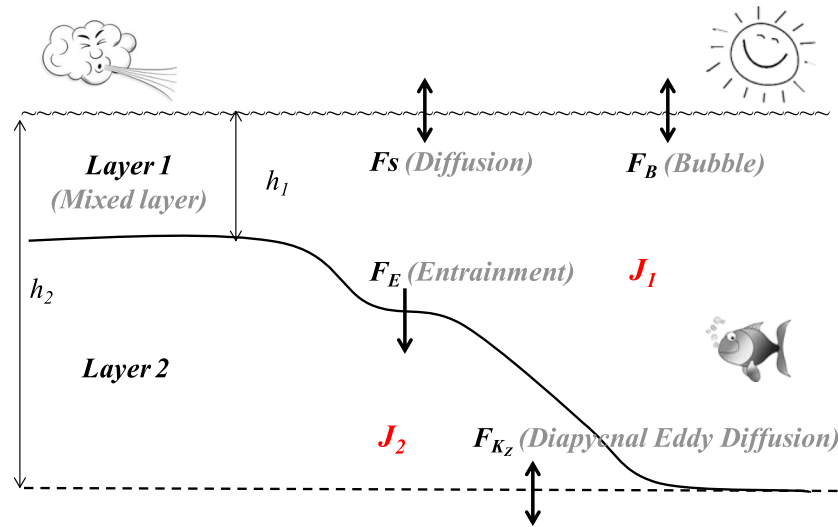
Figure 2. Schematic of upper water column oxygen mass balance model. The first layer is the mixed layer. The base of the second layer is defined as the maximum mixed layer depth in winter. Fluxes (F) are from air-sea gas interface exchange by diffusion (F_S) and bubble processes (F_B), entrainment (F_E), and diapycnal eddy diffusion (F_{Kz}). J_1 and J_2 are the fluxes due to net biological production in layers 1 and 2.

$$J_{NCP} = J_1 + J_2 \qquad \text{mol m}^{-2}\text{d}^{-1} \tag{3}$$

Gas exchange between water and air is modeled as the sum of the air-sea interface exchange, F_S, and bubble processes, F_B. The air-sea interface flux is calculated from equation (4), where k_s is the mass transfer coefficient, $[O_2]$ is the float-measured oxygen concentration, and $[O_2]^{sat}$ is the oxygen saturation calculated from float-measured temperature (T) and salinity (S) [*Garcia and Gordon*, 1992].

$$F_S = F_S\big([O_2] - [O_2]^{sat}\big) \qquad \text{mol m}^{-2}\ \text{d}^{-1} \tag{4}$$

The mass transfer coefficient for air-sea portion of the exchange has been determined by atmospheric eddy correlation measurements of dimethyl sulfide (DMS) [*Goddijn-Murphy et al.*, 2016] (see section 3.7 for an elaboration of this term). The bubble injection flux (F_B), is assumed to be the sum of two mechanisms: one of which involves bubbles that are small enough to entirely collapse (F_c), and the other, F_p, for larger bubbles that exchange gas with the surrounding water and then resurface [*Fuchs et al.*, 1987].

$$F_B = F_c + F_p \qquad \text{mol m}^{-2}\ \text{d}^{-1} \tag{5}$$

F_c is modeled as the product of a mass transfer coefficient (k_c) times the atmospheric mole fraction of oxygen (X^{O_2}).

$$F_c = k_C X^{O_2} \qquad \text{mol m}^{-2}\ \text{d}^{-1} \tag{6}$$

The gas flux across larger bubbles is the product of a second bubble-induced mass transfer coefficient, k_p, and the concentration difference between the oxygen concentration at equilibrium with the enhanced atmospheric pressure inside the bubbles, ΔP, that are subducted below the surface.

$$F_p = -k_p\big\{(1 + \Delta P)[O_2]^{sat} - [O_2]\big\} \qquad \text{mol m}^{-2}\ \text{d}^{-1} \tag{7}$$

In a previous study [*Emerson and Bushinsky*, 2016] multiple air-sea gas flux parameterizations from different bubble models were compared with noble gas data and long-term N_2 measurements on the OSP mooring. The model from *Liang et al.* [2013] proved to match the data best and will be used for this study. Details of this parameterization are presented in *Liang et al.* [2013] and *Emerson and Bushinsky* [2016].

Entrainment of water from below the mixed layer, F_E, is calculated as a product of the mixed layer deepening rate (dh/dt, m d^{-1}) and the vertical O_2 concentration difference ($\Delta[O_2]_{h1}$) at the base of the mixed layer (equation (8)).

$$F_E = \frac{dh}{dt}\Delta[O_2]_{h_1} \qquad \text{mol m}^{-2}\ \text{d}^{-1} \qquad (8)$$

When the mixed layer is deepening the sign of the entrainment flux depends on the concentration gradient between layers 1 and 2. There is no flux to the mixed layer when the mixed layer shoals.

For this simplified two-layer model, the diapycnal eddy diffusion flux F_{Kz} is considered only at the base of the deeper layer because this is the boundary used to define the ANCP. This flux is a function of diapycnal diffusivity coefficient, K_z, and the O_2 concentration gradient, $d[O_2]/dz$ across the base of layer 2.

$$F_{K_z} = K_z\left(\frac{d[O_2]}{dz}\right)_{h_2} \qquad \text{mol m}^{-2}\ \text{d}^{-1} \qquad (9)$$

All float data (temperature, salinity, and oxygen concentration) were interpolated into a 1 day interval with a depth resolution of 1 m for the annual mass balance calculation. For each time step, the fluxes described above were calculated and net biological oxygen production (J_{NCP}) was derived by using equations (1)–(3). The cumulative J_{NCP} over a year is converted to ANCP by using an oxygen carbon ratio of 1.45 [*Hedges et al.*, 2002]. The time step in this study was set to be 1 day; decreasing the time step did not alter the ANCP result.

In this study, the parameterization (k_c and k_p) of air-sea exchange through bubble process was optimized based on our N_2 measurements at OSP. The details can be found in section 3.4. An upper limit for the diapycnal eddy diffusion coefficient (K_z) was estimated by using measured oxygen gradients at the winter mixed layer depth and assuming an oxygen utilization rate (OUR) below this depth (see section 3.5 for detail).

An error analysis of the ANCP calculation was performed by using Monte Carlo method. From our previous work [*Bushinsky and Emerson*, 2015], the main uncertainties were determined to be the degree of oxygen supersaturation in the mixed layer, $\Delta[O_2]$; three gas exchange mass transfer coefficients (k_S, k_c, and k_p); and diapycnal diffusivity coefficient (K_z). Randomly distributed errors with carefully determined ranges of uncertainties were introduced in the model, and 2000 iterations were run for each variation in the coefficients. The details of how uncertainty ranges were determined can be found in sections 3.4–3.6.

3. Results and Discussion

3.1. Atmospheric Calibration of SOS-Argo Oxygen Measurements

The air calibration results of SOS-Argo floats are presented in Figure 3. The intercept of regression line is the offset between optode air measurements and pO_2 at time zero, and the slope of the regression line is the drift rate during the deployment. Linear regressions and error estimates are presented in Table 1. The OSP float (F8397) with the longest record of 4 years has a drift rate of −0.36% yr^{-1}. The South Pacific float (F8485) has a drift rate of −0.14% yr^{-1}, over a period of 2.5 years. The three western North Pacific floats (F9294, F9305, and F9306), however, increased in sensitivity with time during the 1.5 year deployment, with drift rates of 0.28, 0.18, and 0.08% yr^{-1}. The time zero offsets and drift rates were applied to the raw float data for correction. The uncertainty of the atmospheric calibration of the oxygen sensors was estimated from the Student's t test and the standard error of the mean of the time series measurements (see Table 1). The standard error of the regression line is smallest at the midpoint of the time series and largest at the ends. To be conservative we use the end values, which have standard errors under ±0.1% using a 67% confidence interval and about ±0.15% using a 95% confidence interval (Table 1). We adopt an uncertainty of ±0.1% for the air-sea oxygen supersaturation, which is the most important measured term in the oxygen mass balance. This value is consistent with uncertainties used in previous SOS-Argo float oxygen mass balance studies [*Bushinsky and Emerson*, 2015; *Bushinsky et al.*, 2016]. We shall see in section 3.7 that minimizing the error on the oxygen supersaturation measurement by using air calibration is essential for determining accurate values of ANCP.
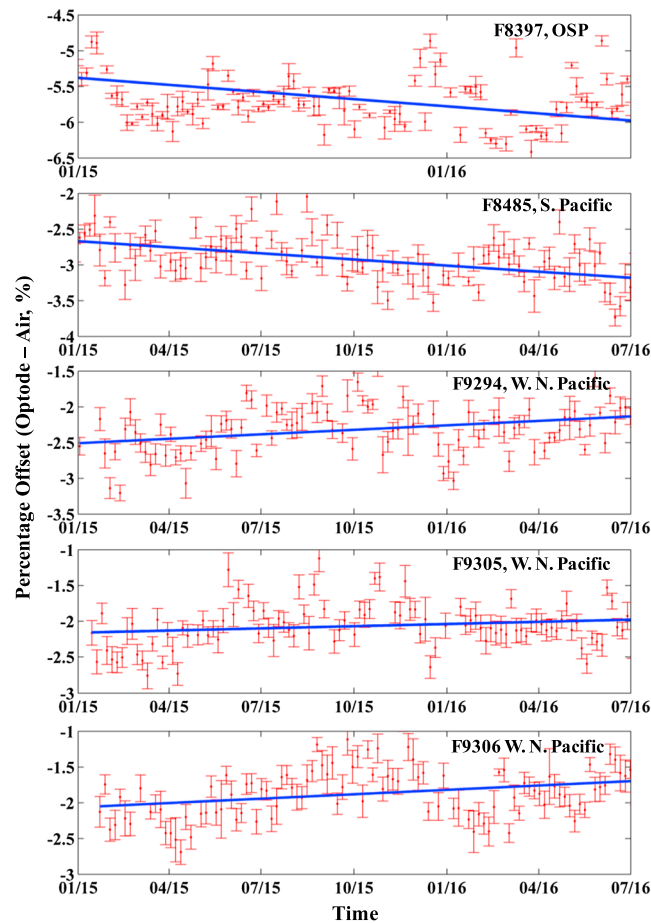
Figure 3. Percentage offset between oxygen sensor pO_2 measurement in air and the pO_2 calculated from atmospheric pressure and the oxygen mole fraction, $(pO_2^{optode} - pO_2^{air})/pO_2^{air} \times 100\%$ for five SOS-Argo floats. Linear regressions (in blue lines, see detail in Table 2) incorporate all available data; only the period from January 2015 to July 2016 was displayed in the above figure. The error bars represent the standard deviation around the mean for 20–30 measurements during each air measurement period.

3.2. Calibration of MBARI Argo Measurements

Since the MBARI float (F8497) continued moving away from HOT, there were just 11 pairs of Winkler and float-derived oxygen data in the top 200 m of water column available from February 2013 to December 2014, with an average offset (float-Winkler) of 3.9% (data not shown). A linear fit to the data yielded the following equation for correction the Optode data to titration measurements: $[O_2]_{corr} = 1.2272 \times [O_2]_{optode} - 57.58$ ($R^2 = 0.96$, $n = 11$). The MBARI float (F8497) continued moving away from HOT (Figure S1, bottom), so we only choose the data within 300 km from HOT for this calibration. Details of this calibration procedure are presented in the supporting information.

3.3. Oxygen Supersaturation

The evolution of oxygen supersaturation in the upper water column (0–150 m) for five floats in subtropical Pacific and subarctic OSP is presented in Figure 4. The solid black line indicates the mixed layer depth, which is often defined by a density offset from the value at 10 m by using a threshold of 0.03 kg m^{-3} [De Boyer Montégut et al., 2004]. However, to match the uniform oxygen concentration distribution in the mixed

layer, we use a larger threshold of 0.18 kg m^{-3} for the subtropical floats (see the supporting information for details). The mixed layer depth probably varies on a daily time scale (maybe diurnally); however, for our purpose we need the deepest value over the period of the gas exchange residence time of about 1 week. For the three western North Pacific floats (Figures 4a–4c), one eastern North Pacific float (Figure 4d), and the OSP float in the subarctic North Pacific (Figure 4f), the mixed layer started shoaling/deepening on April and November, respectively. Correspondingly, oxygen in the mixed layer was supersaturated from mid-April to November and near saturation or slightly undersaturated for the rest of the year. For the South Pacific float (Figure 4e), the mixed layer started shoaling/deepening on July and January, respectively. Most of the year oxygen in the mixed layer was near saturation or undersaturated, with the lowest oxygen supersaturation observed from mid-June to mid-September.

3.4. Optimization of Air-Sea Gas Exchange Model for Bubble Process

In order to optimize the gas exchange model for bubble processes (including F_c and F_p), a mixed layer nitrogen mass balance calculation was carried out to recreate the nitrogen evolution at OSP from June 2012 to June 2013 and compared with the measured surface water nitrogen concentrations from GTD on the OSP mooring. The same model used for oxygen was used for nitrogen (equation (1)) except that $J = 0$. [N$_2$] values below the mixed layer are necessary to calculate the entrainment flux, but the data are only for the surface waters. Deeper values were set to equal the saturation concentrations

Table 1. SOS Argo Float-Derived Oxygen Uncertainty and Drift Estimates From Air Calibration[a]

| Float | Deployment Days | Number of Air Periods (n) | Student's t Uncertainty ($t_{(1-q/100)[n]} \times s_{\hat{Y}}$ (%)) | | Accuracy, b (%) | Drift Rate, a (%/yr) |
			95% Conf.	67% Conf.		
F8397	1490	134	0.16	0.08	-4.45 ± 0.17	-0.36 ± 0.06
F8485	925	117	0.12	0.06	-2.66 ± 0.23	-0.14 ± 0.13
F9294	560	102	0.13	0.07	-2.52 ± 0.13	0.28 ± 0.14
F9305	545	101	0.12	0.06	-2.17 ± 0.12	0.18 ± 0.14
F9306	540	103	0.13	0.07	-1.95 ± 0.14	0.08 ± 0.16

[a]The Student's t confidence interval from tables is $t(1-q/100)[n] \times s_{\hat{Y}i}$, where q is either 95 or 67 and n is the number of measurements. The standard error is $s_{\hat{Y}i} = \sqrt{s_{Y\cdot X}^2 \left[\frac{1}{n} + \frac{(X_i - \overline{X})^2}{\sum (X_i - \overline{X})^2} \right]}$, where $s_{Y\cdot X}^2 = \frac{\sum (Y - \hat{Y})^2}{n-2}$. The linear regression lines through the air calibration data in Figure 3 are given by $Y = ax + b$, where Y is the percentage offset between measured pO_2 and the value in air, $(pO_2^{optode} - pO_2^{air})/pO_2^{air} \times 100\%$ and x is the time since deployment. Uncertainties in Y (in units of $\pm$ percent difference between air and water) are presented using the Student's t distribution for both 95% and 67% confidence intervals as calculated from the equations in the footnotes [*Sokal and Rohlf*, 1995]. Uncertainties in Y are greater at the ends of the lines than in the middle of the time series, and we present only the largest uncertainties to be conservative. The final two columns are the offset in accuracy extrapolated to the time of deployment, b, and the slope of the line, or the drift, a, in %/yr.

calculated by using salinity and temperature from the Argo float as it has been shown previously that nitrogen concentrations below the mixed layer are close to saturation [*Emerson et al.*, 1991b]. All terms on the right side of equation (1) were calculated to obtain a time rate of change, $d[N_2]/dt$ that was evaluated relative to the measurements. Since we are focusing on the model prediction of bubble processes we chose to compare data and model results from a time period with high winds when bubble processes were strong (14 December 2012 to 25 March 2013). The values of the bubble mass transfer coefficients, k_c and k_p (equations (6) and (7) in section 2.2), suggested in the model of *Liang et al.* [2013] were varied by applying correction factors (β) to the bubble mass transfer coefficients of the L13 model: $k_c = \beta \times k_c$ (L13), $k_p = \beta \times k_p$ (L13), to obtain the smallest residual between the modeled and measured nitrogen concentrations. Since we could solve for just one variable, we assumed the ratio of k_c and k_p to be the same as determined from the model of *Liang et al.* [2013]. The results of modeled and measured mixed layer [N$_2$] with different correction factors (β) applied to k_c and k_p from *Liang et al.* [2013] are presented in Figure 5 and indicate a best fit (with the smallest residual between the modeled and measured nitrogen concentrations) of $\beta = 0.53$. We adopt this value as the best estimates for k_c and k_p for our NCP calculation. In the Monte Carlo error analysis, which follows later in the paper, we assume that our N$_2$-calibrated estimate of the bubble mass transfer coefficients is a lower limit and the L13 parameterization is the upper limit, resulting in an uncertainty of $\pm25\%$ for these terms.

3.5. Estimate of Diapycnal Eddy Diffusion Coefficient and Its Uncertainty

The value of the diapycnal eddy diffusion coefficient, K_z, at the base of the winter mixed layer is difficult to determine because it is a depth region where mixing changes from a very large number in the "mixed layer" to a background value of 1×10^{-5} m^2 s^{-1} as measured by tracer release experiments at a depth of about 300 m in the pycnocline [e.g., *Ledwell et al.*, 1993]. Detailed microstructure measurements in the top of the pycnocline [*Sun et al.*, 2013] suggest that the transition from very high to background mixing takes place over a depth interval of about 20 m. We estimate an upper limit for the value of K_z at the base of the winter mixed layer, h_2, by taking advantage of the fact that there are a growing number of observations of the rate of respiration in the upper thermocline of the ocean and they are in the range of 25 ± 15 µmol O$_2$ kg^{-1} yr^{-1} (see Table 2). To estimate an upper limit for the diapycnal eddy diffusion coefficient, we assume that vertical mixing is the main mechanism of oxygen supply into the upper thermocline from above. This assumption may be wrong as isopycnal transport is an important process of thermocline ventilation, but this assumption is consistent with the upper limit calculation. If advection or isopycnal mixing is also important, then we will have overestimated the diapycnal diffusion coefficient.
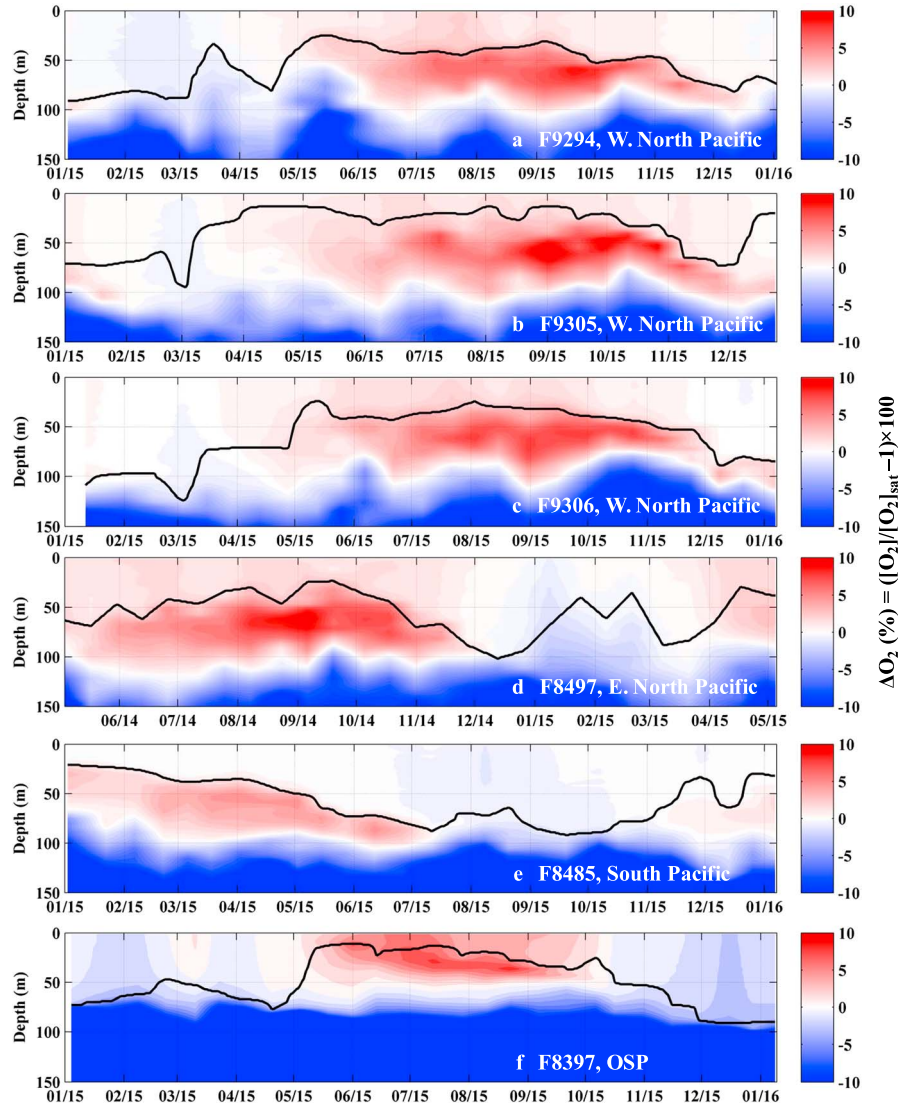
Figure 4. Oxygen supersaturation ΔO_2 (%) = ($[O_2]/[O_2]_{sat}$ − 1) × 100 as a function of depth and time from five SOS-Argo floats in the Pacific Ocean. The solid black line indicates mixed layer depth.

At steady state the integrated respiration rate, the oxygen utilization rate (OUR, mol m^{-3} s^{-1}), over the depth interval from high to low mixing ($z = h_2$ and $h_2 + 20$, respectively) is equal to the flux from above ($F_{Kz,h2}$) minus the flux at the bottom of the region ($F_{Kz,h2 + 20}$):

$$\int_h^{h+20} OUR\, dz = F_{k_z,h_2} - F_{k_z,h_2 + 20}$$

$$= K_{z,h_2}\left(\frac{d[O_2]}{dz}\right)_{h_2} - K_{z,h_2 + 20}\left(\frac{d[O_2]}{dz}\right)_{h_2 + 20} \qquad \text{mol m}^{-2}\ \text{s}^{-1} \qquad (10)$$

The respiration rate range 25 ± 15 μmol O$_2$ kg^{-1} yr^{-1}(see Table 2 for details) is combined with measured depth gradients of oxygen in equation (10) to determine the $K_{z,h2}$ values at the SOS-Argo float locations (Table 2). The calculation yields an upper limit for $K_{z,h2}$ of 2.0–6.0 × 10^{-5} m^2 s^{-1} at six different locations. We used the midpoint of background K_z value (1.0 × 10^{-5}) [Whalen et al., 2012] and the upper limits calculated in Table 2 in the mass balance model. For floats at OSP (F8397) and South Pacific (F8485), the midpoint K_z values are 1.5 × 10^{-5} and 2.3 × 10^{-5} m^2 s^{-1}, respectively. For those four floats at HOT and western North Pacific, the midpoint K_z value is 3.5 × 10^{-5} m^2 s^{-1}. For the error analysis we assume that the uncertainties of
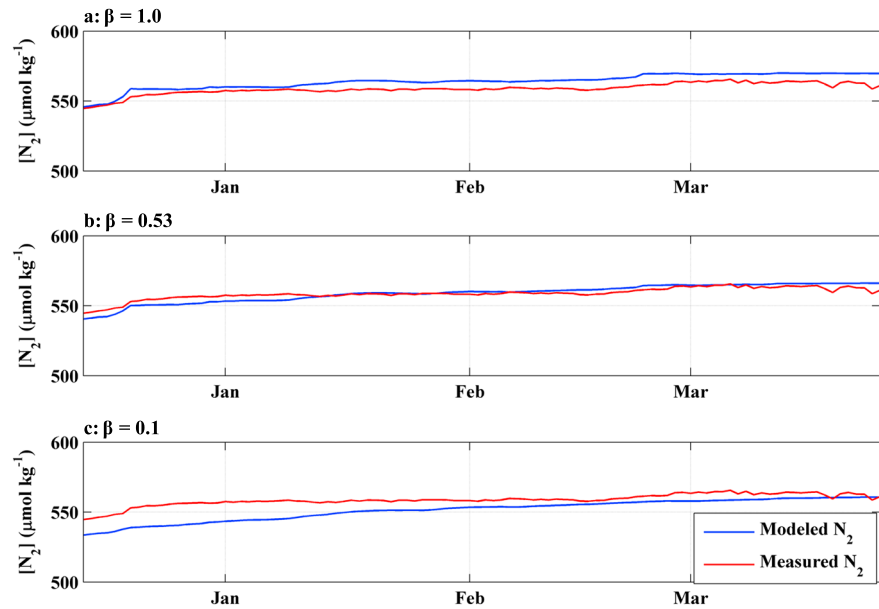
Figure 5. Modeled and measured mixed layer N_2 concentration during the winter of 2012 to 2013 at Ocean Station Papa (OSP). Data are from GTD and O_2 measurements [see *Bushinsky and Emerson*, 2015], and modeled values are from the gas exchange model of *Liang et al.* [2013] (L13). (a–c) The modeled result with different correction factors (β) applied to the bubble mass transfer coefficients of the L13 model: $k_c = \beta \times k_c$ (L13), $k_p = \beta \times k_p$ (L13). The best fit to the data is with the bubble exchange coefficients decreased by about 50%.

K_z are the values necessary to span the range between the upper and lower limit values, which results in errors for K_z of between ±34% and ±71% (Table 2).

3.6. ANCP Calculated From Oxygen Profiles and Upper Water Column Mass Balance Model

Since we use a somewhat different model here than that used in *Bushinsky and Emerson* [2015] (hereinafter B15) we demonstrate consistency with our previous work on this subject by calculating ANCP with the same Argo data used in *Bushinsky and Emerson* [2015] (Table 3A). The model used in B15 has a mixed layer and a series of 1-meter-thick layers to 150 meters with vertical eddy diffusion between all layers. The vertical eddy diffusion coefficient (K_z) at the base of the mixed layer was determined from heat/salt budget measurements at OSP [*Cronin et al.*, 2015], and this value decreases with depth as prescribed by *Sun et al.* [2013]. In contrast, for the simplified two-layer model used in this study (hereinafter Y17) vertical eddy diffusion is considered only at the base of the second layer, with a constant value determined by the methods described above (e.g., 1.5×10^{-5} m^{-2} s^{-1} at OSP, see section 3.5 and Table 2). With the same k_s, k_c, and k_p parameterizations and a constant K_z value of 10^{-5} m^{-2} s^{-1}, our analysis yields an ANCP of 0.4 mol C m^{-2} yr^{-1}, which is identical to the result from B15 (Table 3A, row 1). We discovered after the publication of *Bushinsky and Emerson* [2015]

Table 2. Estimate for the Diapycnal Eddy Diffusion Coefficient at the Base of the Winter Mixed Layer and the Uncertainty of This Value[a]

Float	Location	$\left(d[O_2]/dz\right)_{h_2}$ (mol m^{-4})	$\left(d[O_2]/dz\right)_{h_2+20}$ (mol m^{-4})	$K_{z,h2}$ (m^2 s^{-1})	$K_z = 1/2(K_{z,h2+20} + K_{z,h2})$ (m^2 s^{-1})	K_z (Uncertainty)
F8397	OSP	2.1×10^{-3}	2.7×10^{-3}	2.0×10^{-5}	1.5×10^{-5}	± 34%
F8485	South Pacific	0.6×10^{-3}	0.6×10^{-3}	3.5×10^{-5}	2.3×10^{-5}	± 56%
F8497	HOT	0.3×10^{-3}	0.1×10^{-3}	6.3×10^{-5}	3.7×10^{-5}	± 73%
F9294	Western North	0.3×10^{-3}	0.1×10^{-3}	5.7×10^{-5}	3.3×10^{-5}	± 70%
F9305	Pacific	0.3×10^{-3}	0.2×10^{-3}	5.7×10^{-5}	3.3×10^{-5}	± 70%
F9306		0.3×10^{-3}	0.3×10^{-3}	6.0×10^{-5}	3.5×10^{-5}	± 71%

[a]The upper limit, $K_{z,h2}$, is derived from equation (10), where the integrated respiration rate, in the 20 m layer below the winter mixed layer depth (h_2), $\int_{h_2}^{h_2+20}$OUR dz, is 25 ± 15 µmol O_2 kg^{-1} yr^{-1}. This value is the mean of five separate estimates of AOU divided by the water tracer age in the top of the thermocline from different areas of the ocean (*Sonnerup et al.* [2013, 2015], 16 and 9–25 µmol O_2 kg^{-1} yr^{-1}, respectively; *Stanley et al.* [2012], 15 µmol O_2 kg^{-1} yr^{-1}; *Kadko* [2009], 60 µmol O_2 kg^{-1} yr^{-1}; and *Jenkins* [1998], 30 µmol O_2 kg^{-1} yr^{-1}). Columns 3 and 4 are the measured oxygen gradients at h_2 and $h_2 + 20$ m. $K_{z,h2}$ (column 5) is calculated assuming a value for $K_{z,h2+20} = 1 \times 10^{-5}$ m^2 s^{-1} (see text). The mean K_z values between that calculated at h_2 and assumed at $h_2 + 20$ is in column 6, and the estimated uncertainties (column 7) are the ranges between the upper and lower limits.

Table 3. (A) Comparison of ANCP Calculated at OSP (2012–2013) Using the Same Data From Float F8397 and the Models of *Bushinsky and Emerson* [2015] (B15) and That Used Here (Y17), and (B) ANCP in the Pacific Ocean Using Data From the Other Floats Described in This Paper Calculated From the Y17 Model Described Here[a]

A				
O_2 data	Model	Kz (Parameterization)	Kc and Kp (Optimization)	ANCP (mol C m^{-2} yr^{-1})
Uncorrected	B15	OSP Heat/Salt Budget		0.7 ± 0.5
	B15	10^{-5} m^{-2} s^{-1}	–	0.4 ± 0.5
	Y17			0.4 ± 0.6
Corrected	B15	10^{-5} m^{-2} s^{-1}	–	1.1 ± 0.5
	Y17			1.2 ± 0.6
Corrected	B15	OSP Heat/Salt Budget	–	1.3 ± 0.5
	Y17	1.5×10^{-5} m^{-2} s^{-1}		1.4 ± 0.6
Corrected	B15	OSP Heat/Salt Budget	$\beta = 0.29$	2.4 ± 0.5
	Y17	1.5×10^{-5} m^{-2} s^{-1}	$\beta = 0.53$	2.4 ± 0.6

B			
Location	Float	Year	ANCP (mol C m^{-2} yr^{-1})
Subarctic North Pacific (OSP)	F8397	2015–2016	2.2 ± 0.6
Eastern Subtropical North Pacific (HOT)	F8497[b]	2014–2015	2.4 ± 0.6
Western Subtropical North Pacific	F9294 F9305 F9306	2015–2016	2.2 ± 0.3 2.0 ± 0.3 2.4 ± 0.3
Subtropical South Pacific	F8485	2014–2015 2015–2016	0.6 ± 0.3 0 ± 0.3

[a]See text for detailed explanation of the values in the different rows.
[b]F8497 is a MBARI Argo float without air-calibration mechanism.

that there was an error in the accuracy and drift correction in calculation of oxygen concentration. This resulted in the oxygen concentration at the beginning of the deployment being 0.2% too low and the value after 1 year being 0.3% too low. With the corrected oxygen concentrations, ANCP determined with B15 and Y17 are 1.1 and 1.2 mol C m^{-2} yr^{-1}, respectively (Table 3A, row 2). This difference between ANCP values calculated from uncorrected and corrected oxygen data illustrates the extreme sensitivity of ANCP to the measured degree of oxygen supersaturation at OSP. ANCP sensitivity to the value used for K_z, on the other hand, is not very strong given the range of possible values (Table 3A, row 3). Optimizing the bubble parameters in the L13 model by using the measured N_2 values at OSP suggests that the model-predicted bubble-induced supersaturation is too strong. Making this correction to the L13 bubble model in both the models of B15 and Y17 yields the ANCP of 2.4 mol C m^{-2} yr^{-1} (Table 3A, row 4). The reason for the increase in ANCP estimates is that bubble injection of O_2 in winter (when wind speeds are high) makes the same change in dO_2/dt as net community production. If bubble injection rates are lower, then the NCP estimate is higher, and the ANCP estimate increases. Note that the correction factors (β) are different for different models, but the resulting effect on ANCP estimate is nearly the same. The reason for this difference is due to the different methods of treating vertical mixing below the mixed layer in the N_2 models. This result suggests that our correction to the bubble effect is model-dependent. We believe the more detailed approach in B15 is bound to be more accurate, but we have shown here that it does not affect the calculated values of ANCP.

Overall, the comparisons in Table 3A indicate no significant difference in ANCP estimates using B15 and Y17 models and illustrate the importance of accurate measurements of the air-sea pO_2 difference and wintertime bubble processes. With the corrected oxygen data the ANCP of 2012–2013 at OSP reported in *Bushinsky and Emerson* [2015] is corrected from 0.7 to 1.3 mol C m^{-2} yr^{-1}. Furthermore, by applying the correction of L13 bubble coefficients in both B15 and Y17 models, the best estimate of ANCP at OSP from 2012 to 2013 is 2.4 mol C m^{-2} yr^{-1}. The OSP location is probably one of the most sensitive to these processes anywhere in the ocean because wintertime oxygen supersaturation is very close to air equilibrium and wind speeds are extremely strong.
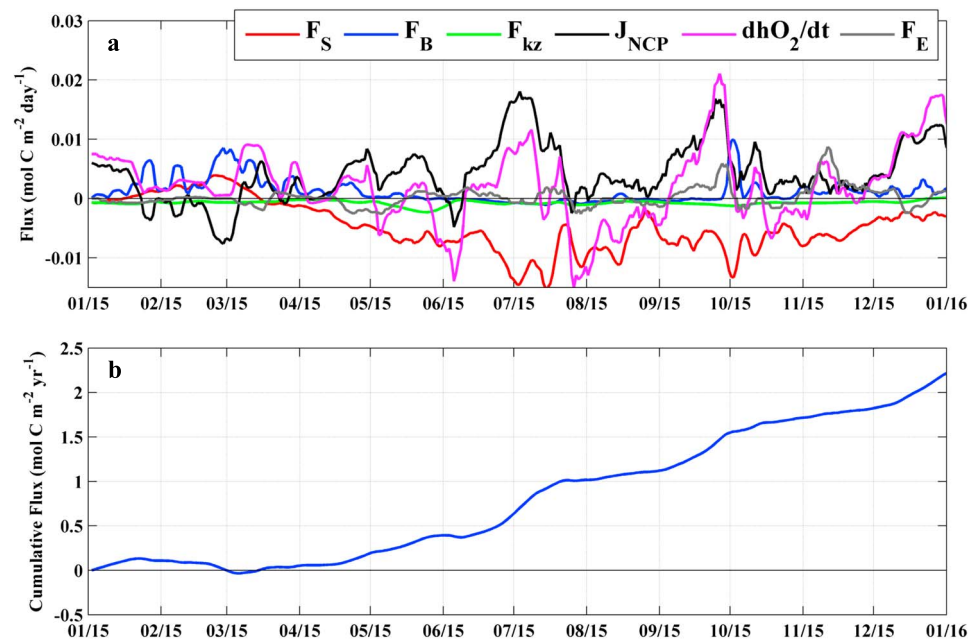
Figure 6. Results of model calculation of ANCP for data from float F9294 in western subtropical North Pacific for the year 2015. (a) Daily carbon fluxes calculated with upper water column oxygen mass balance model. Notice that the dominant terms other than J are dhO2/dt (this is measured), and the gas exchange fluxes F_S and F_B. (b) Cumulative flux (ANCP) derived from daily carbon fluxes. Presented as carbon fluxes using $\Delta O_2/\Delta C = 1.45$ [*Hedges et al.*, 2002].

We applied the Y17 model to annual data from six floats in the Pacific Ocean, using the optimized k_c and k_p values described in section 3.4 and the K_z values described in section 3.5. An example of model output for float F9294 in the western subtropical North Pacific for years 2015–2016 is presented in Figure 6. Figure 6a shows daily variations of each flux in equations (1)–(3). The three most important flux terms, other than net biological production, are the interface air-sea gas flux (F_S), bubble injection (F_B), and the measured time rate of change of oxygen (dh[O$_2$]/dt). From mid-January to mid-March, oxygen in the mixed layer was undersaturated (Figure 6a), causing a positive flux from the atmosphere to the water (Figure 6a). As the seasons progressed to summer oxygen became supersaturated due to a temperature-dependent decrease in solubility and net biological oxygen production. Bubble fluxes were strong during the winter season, when wind speeds frequently exceeded 10 m s^{-1} during winter storms (e.g., March and October). The entrainment flux was significant only during a period of rapid change in mixed layer depth (e.g., May and November; Figure 4a). Diapycnal eddy diffusion plays a small role in gas flux because of the rather low K_z value and the relatively weak O$_2$ concentration gradient at the depth of the winter mixed layer. The model yielded an ANCP of 2.2 mol C m^{-2} yr^{-1} (Figure 6b) for the western subtropical North Pacific.

The ANCP determined from data of the six Argo floats in this study are presented in Table 3B. The ANCP at OSP is determined to be 2.2 mol C m^{-2} yr^{-1}, which is consistent with the results from 2012 (2.5 mol C m^{-2} yr^{-1}) and previous studies (~2.3 mol C m^{-2} yr^{-1} [*Emerson*, 2014]). For the eastern subtropical North Pacific near HOT (F8497), ANCP is 2.4 mol C m^{-2} yr^{-1} for years 2014–2015, which is within the range of previous studies (1.4–3.1 mol C m^{-2} yr^{-1}) based on O$_2$ mass balance [*Emerson et al.*, 2008; *Emerson et al.*, 1995; *Hamme and Emerson*, 2006], carbon isotope [*Brix et al.*, 2006; *Keeling et al.*, 2004; *Quay et al.*, 2009; *Quay et al.*, 2003], and dissolved inorganic carbon drawdown methods [*Lee*, 2001]. In the western subtropical North Pacific, the data from all three floats and model yield an ANCP from 2.0 to 2.4 mol C m^{-2} yr^{-1}, which are very similar to what was observed at HOT in the eastern subtropical North Pacific. Overall, the results from the subtropical North Pacific are consistent with spatial homogeneity of ANCP described by *Emerson* [2014]. However, we found much lower (near-zero) ANCP values in the subtropical South Pacific. The ANCP values are 0.6 and 0 mol C m^{-2} yr^{-1} for years 2014–2015 and 2015–2016, respectively, indicating near metabolic balance over the annual cycle. This is the first value for ANCP determined by mass balance methods that has indicated little or no net carbon production. It is presently based on data from just one SOS-Argo float but suggests the extreme oligotrophic nature of the subtropical South Pacific.

Table 4. Uncertainties for ANCP Calculated by Using Upper Water Column Mass Balance Model[a]

		ANCP Uncertainty (mol C m^{-2} yr^{-1})		
Parameter	Uncertainty (%)	OSPF8397, 2012–2013	Four Subtropical PacificFloats (Except F8497), 2015–2016	Hot, F8497(No Air-Calibration), 2014–2015
$\Delta[O_2]$	±0.1 (±0.3 for F8497)	±0.2	±0.2	±0.6
k_s	±10	±0.15	±0.15	±0.15
k_c and k_p	±25	±0.5	±0.2	±0.2
K_z	±50	±0.2	±0.1	±0.1
Total	–	±0.6	±0.3	±0.6

[a]We considered the four most serious uncertainties (column 1) to be the degree of oxygen supersaturation $\Delta[O_2]$; gas exchange mass transfer coefficients for air-sea diffusive exchange, k_s; small bubble collapse, k_c; large bubble exchange, k_p; and the eddy diffusion coefficient at the base of winter mixed layer, K_z. Column 2 lists the uncertainties explained in the text and other tables. Uncertainties in ANCP for floats in the subarctic Pacific (OSP) and subtropical Pacific determined by the Monte Carlo calculation described in the text are in columns 3–5

3.7. Error Analysis

The most critical factor in the error calculation is assigning the range of uncertainty for the values and coefficients used in the calculation. The most important data term in the mass balance is the value of the degree of oxygen supersaturation. Our methods for evaluating the oxygen error are presented in section 3.1 and Table 1. We concluded that an uncertainty of ±0.1% was appropriate for the measurement of oxygen supersaturation between the air and water on SOS-Argo floats. For MBARI float F8497 at HOT without air-calibration mechanism, the uncertainty was estimated as ±0.3%, by combining the precision of HOT Winkler measurements (± 0.2% accessed in September 2016, http://hahana.soest.hawaii.edu/hot/methods/oxygen.html) and all other potential uncertainties (± 0.1%) from sensor measurements and drift. We will see in Table 4 that even this very low value is still one of the most important errors. The other most significant error is in assessing the accuracy of the bubble flux, which is a model-determined value. Section 3.4 and Figure 5 are devoted to determining the accuracy of the bubble mass transfer coefficients in the model of *Liang et al.* [2013]. We argue that the bubble terms are overestimated in winter based on comparison to N_2 concentration data and assume an error that is ±25%. We believe that the bubble flux is presently the most significant uncertainty in the calculation because it has a great effect on the wintertime results and the error estimate is presently based on a single comparison with N_2 data. The uncertainty in determining the diapycnal eddy diffusion coefficient is outlined in section 3.5 and Table 2. We estimated uncertainties that vary from ±34% to ±73% for the five areas of our study. For the Monte Carlo analysis we used an average of ±50%.

The only important term in the error analysis that has not been discussed is the uncertainty in the air-sea gas transfer coefficient, k_s. We suggest an error of ±10%, which we determined by comparing the three different parameterizations for the bubble-free gas exchange rate. *Goddijn-Murphy et al.* [2016] determined k_s as a function of wind speed based on atmospheric eddy correlation fluxes of dimethyl sulfide (DMS), which is so soluble that it is believed to be unaffected by bubbles. *Woolf* [1997] used the value determined by *Jähne et al.* [1987] in wind tunnel experiments with no visible bubble formation. The third formulation is that of the NOAA Coupled Ocean Atmosphere Response Experiment model [*Fairall et al.*, 2003] used by *Liang et al.* [2013] (L13). At the 10 m wind speed (U_{10}) over the ocean of 6–9 m s^{-1}, the difference in k660 (k_s at a Schmidt number of 660) among these models is about from ±7 to 10%. Since annual mean wind speed values are all around 7 m/s at our subtropical sites, and 8.6 m/s at the subarctic OSP, we use a more conservative ±10% as the uncertainty of k_s.

The Monte Carlo analysis (Table 4) presents the error derived from each of the terms and that estimated from the combination of terms. The results indicate that the uncertainties in oxygen measurement and bubble flux are the most important sources of uncertainties in ANCP estimate. In the subtropical Pacific, compared with SOS-Argo floats, the uncertainty in ANCP is significantly higher for Float 8497 (25% versus 15%), due to the higher uncertainty in oxygen measurements without air-calibration mechanism. With the same Argo data set (F8397 at OSP, June 2012 to June 2013) used in *Bushinsky and Emerson* [2015] at OSP the combined uncertainty is about ±30% of the estimated ANCP. This relative value is higher than that in the western subtropical
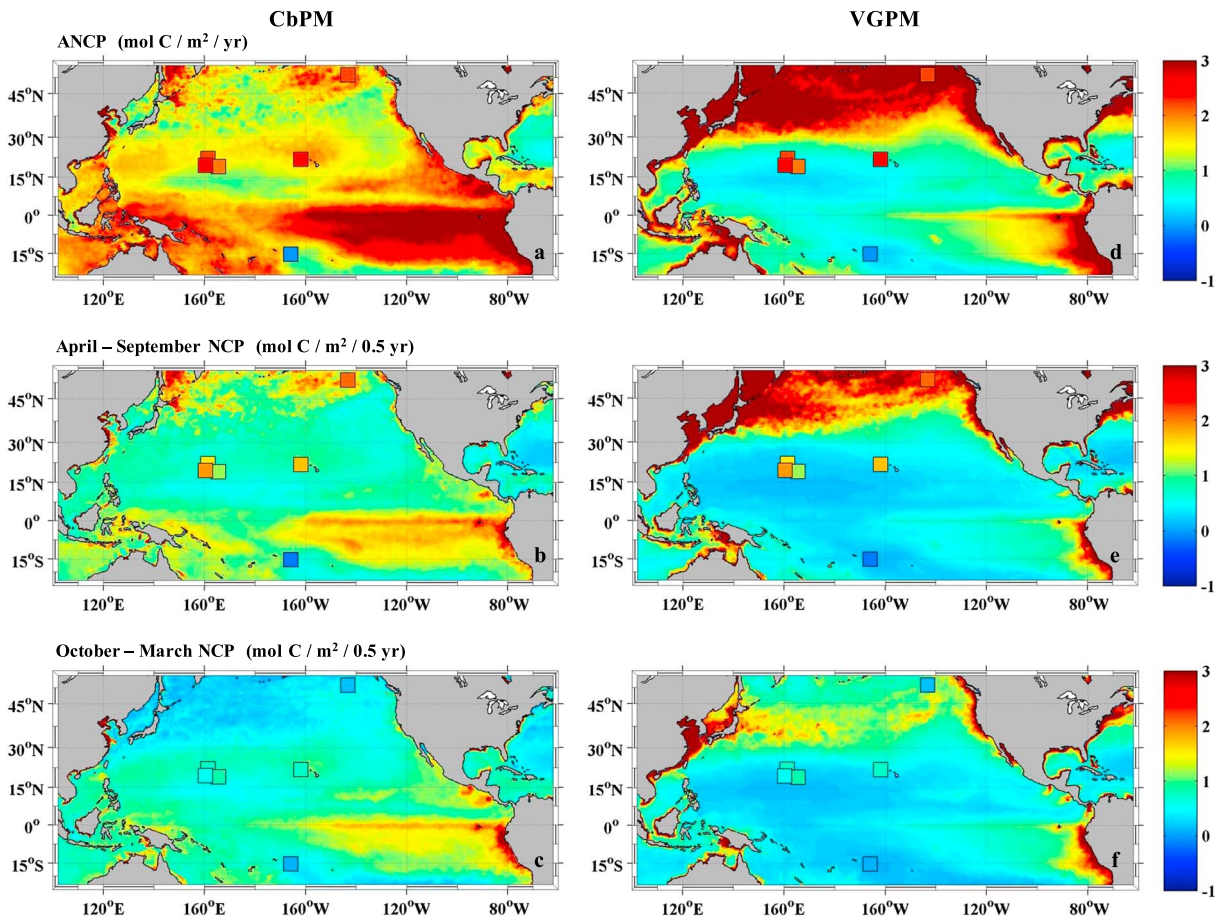
Figure 7. NCP determined by Argo oxygen measurements (colored square) and remote sensing data (background color). (left) Results using CbPM algorithm. (right) Results using VGPM algorithm. Satellite-based NCP was calculated with net primary production (NPP) from CbPM/VGPM algorithms [*Westberry et al.*, 2008; *Behrenfeld and Falkowski*, 1997; http://www.science.oregonstate.edu/ocean.productivity/index.php] multiplied by the NCP/NPP ratio compiled by *Laws et al.* [2011] (equation (11)). (top to bottom) ANCP from January 2015 to January 2016[*], NCP from April to September, NCP from October to March[*]. For the HOT float (F8497) only the 2014–2015 data are available.

ocean (±15%) because of the large error in the bubble flux at OSP due to the much higher winds in the subarctic Pacific. The uncertainty in K_z at OSP is also more important because of the steeper gradient of oxygen at the base of the winter mixed layer. Past estimates of ANCP by oxygen mass balance even when inert gases are measured to experimentally determine the effect of bubbles have been in the range of ±50%, mostly because of uncertainties in the oxygen measurements [*Emerson et al.*, 1991a]. In this study we have shown that in situ measurements of pO_2 with air calibration can bring down the uncertainty in the air-sea oxygen gradient. The new challenge with SOS-Argo measurements will be to minimize the error in the calculation of bubble fluxes at high wind speeds.

3.8. Comparison to Satellite-Based ANCP Estimates

We compare the ANCP values determined here with an estimate of the carbon export determined from satellite-derived NPP and model-derived NCP/NPP ratios. The most widely used NPP algorithms are the Vertically Generalized Production Model (VGPM) and the Carbon Based Production Model (CbPM). VGPM is a "chlorophyll-based" NPP model, for which NPP is a function of chlorophyll, available light, and photosynthetic efficiency [*Behrenfeld and Falkowski*, 1997]. CbPM, on the other hand, is a carbon based NPP model, which relates the satellite estimates of backscattering to phytoplankton carbon biomass [*Westberry et al.*, 2008]. To calculate satellite-derived NCP, NPP determined by the above models is multiplied by the export production to total primary production ratio (ef-ratio) of *Laws et al.* [2011], which relates the ef-ratio to temperature (*T*) and NPP (equation (11)).
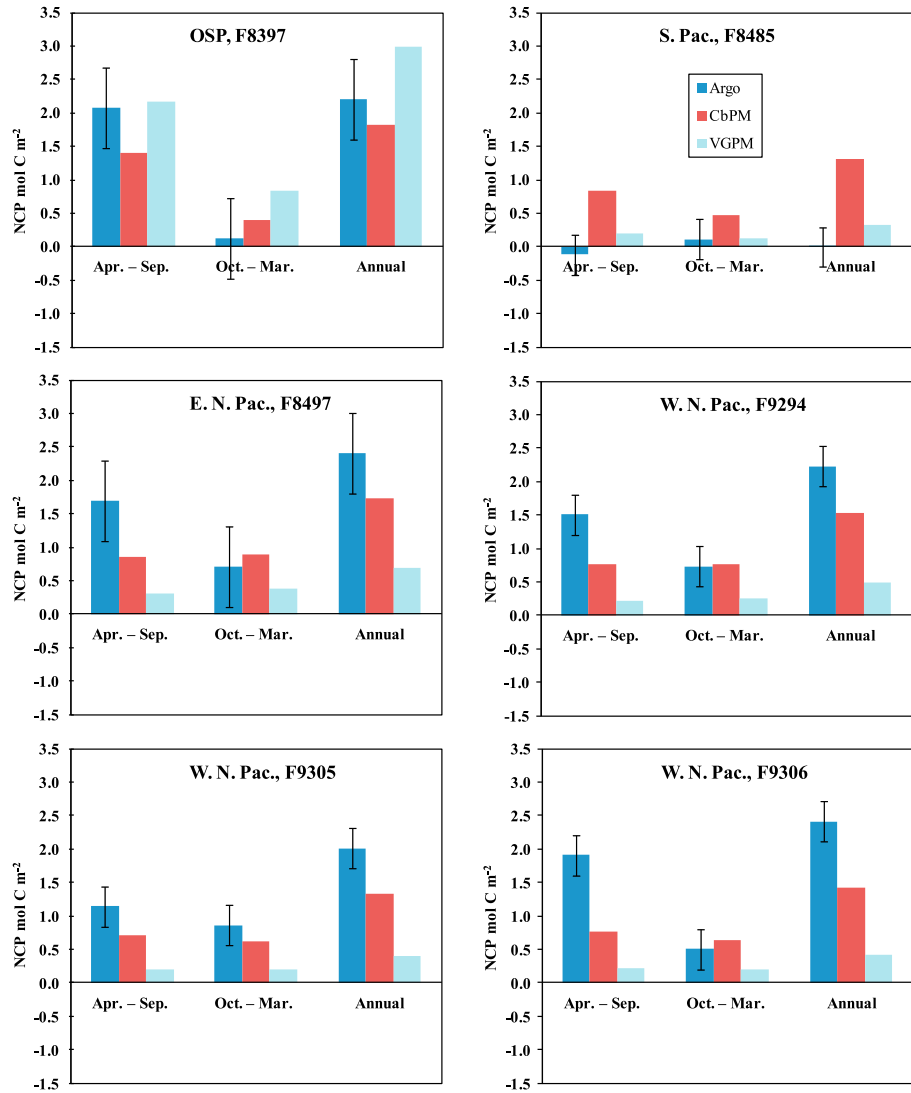
Figure 8. Comparison of NCP derived from Argo oxygen measurements and remote sensing algorithms (CbPM and VGPM). April to September is the more productive summer period for northern hemisphere. The error bars represent uncertainties for the oxygen mass balance-derived NCP (see section 3.7 for details).

$$\text{ef} = 0.04756\left(0.78 - \frac{0.43T}{30}\right)\text{NPP}^{0.307} \tag{11}$$

We chose this ef-ratio because it was parameterized based on measurements of total and export production from a wide range of oceanic habitats, including estimates from the uptake of ^{15}N–labeled nitrate (new production), nutrient drawdown, oxygen/carbon-based estimates of export production, and particle export production from sediment trap or [234]Th measurements.

The results (Figures 7 and 8) indicate that the VGPM algorithm produces much higher estimates of ANCP poleward of 30°, while the CbPM algorithm results in significantly higher ANCP in the subtropical Pacific. In the subarctic North Pacific at OSP for years 2015–2016, the CbPM algorithm underestimates NCP during the more productive period (April to September), while the VGPM result is similar to the SOS-Argo oxygen measurements. However, during winter (October to March), both VGPM and CbPM algorithms overestimate NCP. The net result is that over the whole year the CbPM algorithm yields an ANCP that is closer to the result from SOS-Argo oxygen measurements and oxygen mass balance model. In the subtropical South Pacific (F8485), the oxygen mass balance-derived result indicates net heterotrophy in the southern hemisphere

winter (April to September), net autotrophy in the summer (October to March), and overall near zero ANCP for years 2015 to 2016. The remote sensing products, however, suggest a pattern with positive annual net export and higher production in the southern hemisphere winter than summer. In this case, the result from VGPM is closer to oxygen mass balance-derived ANCP. Comparisons of satellite-derived ANCP with data from the four floats in the subtropical North Pacific indicate similar seasonal patterns with both oxygen mass balance and remote sensing estimates indicating higher production in the summer. However, the remote sensing estimates of ANCP are always lower than the oxygen mass balance estimates. The CbPM algorithm-predicted ANCP is closer to the mass balance observations than VGPM.

Overall, assuming the same ef-ratio model of *Laws et al.* [2011], the ANCP derived from CbPM NPP algorithm is closer to the value derived from the SOS-Argo oxygen data and mass balance model at the subarctic OSP and subtropical North Pacific, while the difference between ANCP-derived from the VGPM NPP algorithm and SOS-Argo oxygen measurements is smaller in the subtropical South Pacific. No single-satellite NPP algorithms can reproduce the export production estimated from Argo oxygen measurements across the Pacific. This conclusion is similar to that in the recent comparison made by *Palevsky et al.* [2016a] for the subtropical subarctic boundary. Furthermore, as pointed out by *Palevsky et al.* [2016a], different choices of ef-ratio will also affect the result of satellite-based ANCP estimates. Comparisons of satellite-derived and GCM-produced ANCP with results of mass balance measurements are still very crude because of the scarcity of experimental measurements and the different definitions of the upper ocean for different approaches. The way forward will be to use the comparison between output of GCMs that include ecosystems and metabolite concentrations with results of mass balance measurements to derive more accurate distributions of global variations. These values can then be used to tune the remote sensing algorithms. Achieving this goal will require a much wider distribution of mass balance ANCP measurements.

4. Summary and Conclusions

Continuous oxygen measurements make it possible to determine the flux of biologically produced oxygen out of the upper ocean and infer by stoichiometry the flux of carbon that escapes to the thermocline over the period of a year: the annual net community production (ANCP). With the oxygen measurements from Argo profiling floats and an upper water column oxygen mass balance model, ANCP was determined in the historically undersampled subtropical western North Pacific and South Pacific. In the western subtropical North Pacific, the ~2 mol C m^{-2} yr^{-1} estimates of ANCP are the same, within our error, to previous mass balance measurements at eastern North Pacific (HOT). Results from the subtropical South Pacific were determined to be indistinguishable from zero, which is the first value for ANCP from mass balance methods that have indicated little or no net carbon production.

The largest uncertainties in ANCP calculated from O_2 mass balance are from the measurement of the air-sea O_2 gradient and the calculation of the gas exchange effect of bubbles in winter. We have been able to improve the accuracy of the float-measured pO_2 difference between the air and the water to a few tenths of 1% using in situ air calibrations. This improvement reduces the uncertainty of the oxygen mass balance estimate of ANCP from ±50% [*Emerson et al.*, 1991b] to ± ~30%.

Comparisons with satellite-based ANCP estimates indicated that the oxygen mass balance experimental results yielded values higher than satellite estimates in the subtropical North Pacific but lower in the subtropical South Pacific. Continuous geochemical tracer measurements like SOS-Argo oxygen measurements presented here will be necessary to refine both global model and the remote sensing algorithms for predicting accurate ANCP and biological carbon export over large temporal and spatial scales.

References

Behrenfeld, M. J., and P. G. Falkowski (1997), Photosynthetic rates derived from satellite-based chlorophyll concentration, *Limnol. Oceanogr.*, *42*(1), 1–20.

Bopp, L., P. Monfray, O. Aumont, J. L. Dufresne, G. Le Treut, G. Madec, L. Terray, and J. C. Orr (2001), Potential impact of climate change on marine export production, *Global Biogeochem. Cycles*, *15*(1), 81–99, doi:10.1029/1999GB001256.

Brix, H., N. Gruber, D. M. Karl, and N. R. Bates (2006), On the relationships between primary, net community, and export production in subtropical gyres, *Deep Sea Res., Part II*, *53*(5), 698–717.

Bushinsky, S. M., and S. Emerson (2015), Marine biological production from in situ oxygen measurements on a profiling float in the subarctic Pacific Ocean, *Global Biogeochem. Cycles*, *29*, 2050–2060, doi:10.1002/2015GB005251.

Bushinsky, S. M., S. R. Emerson, S. C. Riser, and D. D. Swift (2016), Accurate oxygen measurements on modified Argo floats using in situ air calibrations, *Limnol. Oceanogr.*, *14*, 491–505, doi:10.1002/lom3.10107.

Craig, H., and T. Hayward (1987), Oxygen supersaturation in the ocean: Biological versus physical contributions, *Science*, *235*(4785), 199–202.

Cassar, N., S. W. Wright, P. G. Thomson, T. W. Trull, K. J. Westwood, M. Salas, A. Davidson, I. Pearce, D. M. Davies, and R. J. Matear (2015), The relation of mixed-layer net community production to phytoplankton community composition in the Southern Ocean, *Global Biogeochem. Cycles*, *29*, 446–462, doi:10.1002/2014GB004936.

Cronin, M. F., N. A. Pelland, S. R. Emerson, and W. R. Crawford (2015), Estimating diffusivity from the mixed layer heat and salt balances in the North Pacific, *J. Geophys. Res. Oceans*, *120*, 7346–7362, doi:10.1002/2015JC011010.

de Boyer Montégut, C., G. Madec, A. S. Fischer, A. Lazar, and D. Iudicone (2004), Mixed layer depth over the global ocean: An examination of profile data and a profile-based climatology, *J. Geophys. Res.*, *109*, C12003, doi:10.1029/2004JC002378.

DeVries, T., and C. Deutsch (2014), Large-scale variations in the stoichiometry of marine organic matter respiration, *Nat. Geosci.*, *7*(12), 890–894.

Emerson, S. (2014), Annual net community production and the biological carbon flux in the ocean, *Global Biogeochem. Cycles*, *28*, 14–28, doi:10.1002/2013GB004680.

Emerson, S., and S. Bushinsky (2016), The role of bubbles during air-sea gas exchange, *J. Geophys. Res. Oceans*, *121*, 4360–4376, doi:10.1002/2016JC011744.

Emerson, S., and C. Stump (2010), Net biological oxygen production in the ocean—II: Remote in situ measurements of O_2 and N_2 in subarctic pacific surface waters, *Deep Sea Res., Part I*, *57*(10), 1255–1265.

Emerson, S., P. Quay, C. Stump, D. Wilbur, and M. Knox (1991), O_2, Ar, N_2, and ^{222}Rn in surface waters of the subarctic ocean: Net biological O_2 production, *Global Biogeochem. Cycles*, *5*(1), 49–69, doi:10.1029/90GB02656.

Emerson, S., P. Quay, C. Stump, D. Wilbur, and R. Schudlich (1995), Chemical tracers of productivity and respiration in the subtropical Pacific Ocean, *J. Geophys. Res.*, *100*(C8), 15,873–15,887, doi:10.1029/95JC01333.

Emerson, S., C. Stump, and D. Nicholson (2008), Net biological oxygen production in the ocean: Remote in situ measurements of O_2 and N_2 in surface waters, *Global Biogeochem. Cycles*, *22*, GB3023, doi:10.1029/2007GB003095.

Fairall, C. W., E. F. Bradley, J. E. Hare, A. A. Grachev, and J. B. Edson (2003), Bulk parameterization of air–sea fluxes: Updates and verification for the COARE algorithm, *J. Clim.*, *16*(4), 571–591.

Fassbender, A. J., C. L. Sabine, and M. F. Cronin (2016), Net community production and calcification from 7 years of NOAA Station Papa Mooring measurements, *Global Biogeochem. Cycles*, *30*, 250–267, doi:10.1002/2015GB005205.

Fuchs, G., W. Roether, and P. Schlosser (1987), Excess ^{3}He in the ocean surface layer, *J. Geophys. Res.*, *92*(C6), 6559–6568, doi:10.1029/JC092iC06p06559.

Garcia, H. E., and L. I. Gordon (1992), Oxygen solubility in seawater: Better fitting equations, *Limnol. Oceanogr.*, *37*(6), 1307–1312.

Garcia, H. E., R. A. Locarnini, T. P. Boyer, J. I. Antonov, O. K. Baranova, M. M. Zweng, J. R. Reagan, and D. R. Johnson (2014), *World Ocean Atlas 2013, Volume 4: Dissolved Inorganic Nutrients (Phosphate, Nitrate, Silicate)*, *NOAA Atlas NESDIS*, vol. 76, edited by S. Levitus and A. Mishonov, p. 25, U.S. Dep. of Commer., Natl. Oceanic and Atmos. Administr. (NOAA), Natl. Environ. Satell., Data, and Inf. Serv. (NESDIS), Silver Spring, Md.

Goddijn-Murphy, L., D. K. Woolf, A. H. Callaghan, P. D. Nightingale, and J. D. Shutler (2016), A reconciliation of empirical and mechanistic models of the air-sea gas transfer velocity, *J. Geophys. Res. Oceans*, *121*, 818–835, doi:10.1002/2015JC011096.

Hamme, R. C., and S. R. Emerson (2006), Constraining bubble dynamics and mixing with dissolved gases: Implications for productivity measurements by oxygen mass balance, *Journal of Marine Research*, *64*(1), 73–95.

Hedges, J. I., J. A. Baldock, Y. Gélinas, C. Lee, M. L. Peterson, and S. G. Wakeham (2002), The biochemical and elemental compositions of marine plankton: A NMR perspective, *Mar. Chem.*, *78*(1), 47–63.

Hofmann, M., and H.-J. Schellnhuber (2009), Oceanic acidification affects marine carbon pump and triggers extended marine oxygen holes, *Proc. Natl. Acad. Sci. U.S.A.*, *106*(9), 3017–3022, doi:10.1073/pnas.0813384106.

Jähne, B., K. O. Münnich, R. Bösinger, A. Dutzi, W. Huber, and P. Libner (1987), On the parameters influencing air-water gas exchange, *J. Geophys. Res.*, *92*(C2), 1937–1949, doi:10.1029/JC092iC02p01937.

Jenkins, W. J. (1998), Studying subtropical thermocline ventilation and circulation using tritium and ^{3}He, *J. Geophys. Res.*, *103*(C8), 15,817–15,831, doi:10.1029/98JC00141.

Kadko, D. (2009), Rapid oxygen utilization in the ocean twilight zone assessed with the cosmogenic isotope ^{7}Be, *Global Biogeochem. Cycles*, *23*, GB4010, doi:10.1029/2009GB003510.

Keeling, C. D., H. Brix, and N. Gruber (2004), Seasonal and long-term dynamics of the upper ocean carbon cycle at Station ALOHA near Hawaii, *Global Biogeochem. Cycles*, *18*, GB4006, doi:10.1029/2004GB002227.

Körtzinger, A., U. Send, R. Lampitt, S. Hartman, D. W. Wallace, J. Karstensen, M. Villagarcia, O. Llinás, and M. DeGrandpre (2008), The seasonal pCO_2 cycle at 49°N/16.5°W in the northeastern Atlantic Ocean and what it tells us about biological productivity, *J. Geophys. Res.*, *113*, C04020, doi:10.1029/2007JC004347.

Kwon, E. Y., F. Primeau, and J. L. Sarmiento (2009), The impact of remineralization depth on the air-sea carbon balance, *Nat. Geosci.*, *2*(9), 630–635, doi:10.1038/ngeo612.

Laws, E. A., E. D'Sa, and P. Naik (2011), Simple equations to estimate ratios of new or export production to total production from satellite-derived estimates of sea surface temperature and primary production, *Limnol. Oceanogr.: Methods*, *9*(12), 593–601.

Ledwell, J. R., A. J. Watson, and C. S. Law (1993), Evidence for slow mixing across the pycnocline from an open-ocean tracer-release experiment, *Nature*, *364*(6439), 701–703.

Lee, K. (2001), Global net community production estimated from the annual cycle of surface water total dissolved inorganic carbon, *Limnol. Oceanogr.*, *46*(6), 1287–1297.

Liang, J. H., C. Deutsch, J. C. McWilliams, B. Baschek, P. P. Sullivan, and D. Chiba (2013), Parameterizing bubble-mediated air-sea gas exchange and its effect on ocean ventilation, *Global Biogeochem. Cycles*, *27*, 894–905, doi:10.1002/gbc.20080.

Longhurst, A. R., and W. G. Harrison (1989), The biological pump: Profiles of plankton production and consumption in the upper ocean, *Prog. Oceanogr.*, *22*(1), 47–123.

Nicholson, D., S. Emerson, and C. C. Eriksen (2008), Net community production in the deep euphotic zone of the subtropical North Pacific gyre from glider surveys, *Limnol. Oceanogr.*, *53*(5part2), 2226–2236.

Palevsky, H. I., P. D. Quay, and D. P. Nicholson (2016a), Discrepant estimates of primary and export production from satellite algorithms, a biogeochemical model, and geochemical tracer measurements in the North Pacific Ocean, *Geophys. Res. Lett.*, *43*, 8645–8653, doi:10.1002/2016GL070226.

Palevsky, H. I., P. D. Quay, D. E. Lockwood, and D. P. Nicholson (2016b), The annual cycle of gross primary production, net community production, and export efficiency across the North Pacific Ocean, *Global Biogeochem. Cycles*, *30*, 361–380, doi:10.1002/2015GB005318.

Plant, J. N., K. S. Johnson, C. M. Sakamoto, H. W. Jannasch, L. J. Coletti, S. C. Riser, and D. D. Swift (2016), Net community production at Ocean Station Papa observed with nitrate and oxygen sensors on profiling floats, *Global Biogeochem. Cycles*, *30*, 859–879, doi:10.1002/2015GB005349.

Quay, P., R. Sonnerup, T. Westby, J. Stutsman, and A. McNichol (2003), Changes in the ^{13}C/^{12}C of dissolved inorganic carbon in the ocean as a tracer of anthropogenic CO_2 uptake, *Global Biogeochem. Cycles*, *17*(1), 1004, doi:10.1029/2001GB001817.

Quay, P., J. Stutsman, R. Feely, and L. Juranek (2009), Net community production rates across the subtropical and equatorial Pacific Ocean estimated from air-sea δ13C disequilibrium, *Global Biogeochem. Cycles*, *23*, GB2006, doi:10.1029/2008GB003193.

Riser, S. C., and K. S. Johnson (2008), Net production of oxygen in the subtropical ocean, *Nature*, *451*(7176), 323–325.

Siegel, D. A., K. O. Buesseler, S. C. Doney, S. F. Sailley, M. J. Behrenfeld, and P. W. Boyd (2014), Global assessment of ocean carbon export by combining satellite observations and food-web models, *Global Biogeochem. Cycles*, *28*, 181–196, doi:10.1002/2013GB004743.

Sokal, R. R., and F. J. Rohlf (1995) *Biometry*, 3rd ed., pp. 466–476, W. H. Freeman and Company, Macmillan, New York.

Sonnerup, R. E., S. Mecking, and J. L. Bullister (2013), Transit time distributions and oxygen utilization rates in the Northeast Pacific Ocean from chlorofluorocarbons and sulfur hexafluoride, *Deep Sea Res., Part I*, *72*, 61–71.

Sonnerup, R. E., S. Mecking, J. L. Bullister, and M. J. Warner (2015), Transit time distributions and oxygen utilization rates from chlorofluorocarbons and sulfur hexafluoride in the Southeast Pacific Ocean, *J. Geophys. Res. Oceans*, *120*, 3761–3776, doi:10.1002/2015JC010781.

Stanley, R. H., S. C. Doney, W. J. Jenkins, and D. E. Lott (2012), Apparent oxygen utilization rates calculated from tritium and helium-3 profiles at the Bermuda Atlantic Time-series Study site, *Biogeosci. Discuss.*, *8*, 9977–10,015.

Sun, O. M., S. R. Jayne, K. L. Polzin, B. A. Rahter, and L. C. S. Laurent (2013), Scaling turbulent dissipation in the transition layer, *J. Phys. Oceanogr.*, *43*(11), 2475–2489.

Teng, Y. C., F. W. Primeau, J. K. Moore, M. W. Lomas, and A. C. Martiny (2014), Global-scale variations of the ratios of carbon to phosphorus in exported marine organic matter, *Nat. Geosci.*, *7*(12), 895–898.

Tomczak, M., and J. S. Godfrey (1994), CHAPTER 8—The Pacific Ocean, in *Regional Oceanography*, pp. 113–147, Pergamon, Amsterdam.

Whalen, C. B., L. D. Talley, and J. A. MacKinnon (2012), Spatial and temporal variability of global ocean mixing inferred from Argo profiles, *Geophys. Res. Lett.*, *39*, L18612, doi:10.1029/2012GL053196.

Westberry, T., M. J. Behrenfeld, D. A. Siegel, and E. Boss (2008), Carbon-based primary productivity modeling with vertically resolved photoacclimation, *Global Biogeochem. Cycles*, *22*, GB2024, doi:10.1029/2007GB003078.

Westberry, T. K., P. J. l. B. Williams, and M. J. Behrenfeld (2012), Global net community production and the putative net heterotrophy of the oligotrophic oceans, *Global Biogeochem. Cycles*, *26*, GB4019, doi:10.1029/2011GB004094.

Wong, C., N. A. D. Waser, Y. Nojiri, F. A. Whitney, J. S. Page, and J. Zeng (2002), Seasonal cycles of nutrients and dissolved inorganic carbon at high and mid latitudes in the North Pacific Ocean during the Skaugran cruises: Determination of new production and nutrient uptake ratios, *Deep Sea Res., Part II*, *49*(24), 5317–5338.

Woolf, D. K. (1997), Bubbles and their role in air-sea gas exchange, in *The Sea Surface and Global Change*, edited by P. S. Liss and R. A. Duce, pp. 173–205, Cambridge Univ. Press, U. K.